Nanoscale

Accepted Manuscript

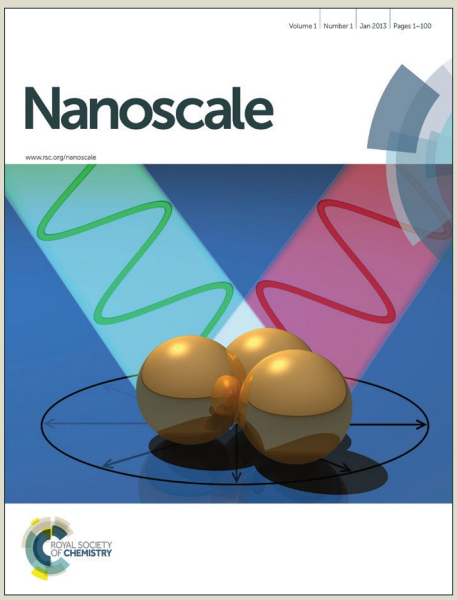

ROYAL SOCIETY OF CHEMISTRY

www.rsc.org/nanoscale

Journal Name

ARTICLE

Received 00th January 20xx,

Accepted 00th January 20xx

DOI: 10.1039/x0xx00000x

www.rsc.org/

Facile Synthesis of Hybrid Nanorods with $Sb_2Se_3/AgSbSe_2$ Heterojunction Structure for High Performance Photodetectors

Shuo Chen[a], Xvsheng Qiao[a], Fengxia Wang[b], Qun Luo[b], Xianghua Zhang[c], Xia Wan[d], Yang Xu[d], Xianping Fan*[,a]

An effective colloidal process involving hot-injection method is developed to synthesize uniform single-crystalline Sb_2Se_3 nanorods with high yields. The photoconductive characteristics of the as-synthesized Sb_2Se_3 nanorods are investigated by developing a film-based photodetector and this device display a remarkable response to visible light with an "ON/OFF" ratio as high as 50 (with an incident light density of 12.05 $mWcm^{-2}$), short response/recovery times and long-term durability. To overcome the challenge of intrinsic low electrical conductivity of Sb_2Se_3, the hybrid nanorods with $Sb_2Se_3/AgSbSe_2$ heterojunction structure with a type-II band alignment is firstly prepared. The electric current of the photodetector based on $Sb_2Se_3/AgSbSe_2$ hybrid nanorods film has been significantly increased both in dark and under light illumination. The responsivity of the photodetector based on $Sb_2Se_3/AgSbSe_2$ hybrid nanorods film is about 4.2 times as much as that of the photodetector based on Sb_2Se_3 nanorods film. This improvement can be considered as an important step to promote Sb_2Se_3 based semiconductors for applications in high performance photodetectors.

Introduction

Binary and ternary chalcogenide materials have drawn tremendous research attention in recent years due to their potential applications in photovoltaic and thermoelectric areas.[1-6] Antimony selenide (Sb_2Se_3) is an important direct narrow band gap semiconductor of group V-VI binary compounds, which is highly anisotropic semiconductor crystallizing in layered structures with layers in parallel to the growth direction.[7] Its useful properties (e.g., photovoltaic, photoconducting, photocatalytic, Peltier effect) make it promising candidate for many important applications in diverse areas such as solar energy conversion, thermoelectric cooling, photodetector technology, thermoelectric power generation, and opto-electronics in the near-infrared region.[8] The Sb_2Se_3 has a high absorption coefficient of 10^5 cm^{-1}. However, the very low electrical conductivity (10^{-6} $\Omega^{-1}m^{-1}$) of the Sb_2Se_3 in bulk state limited its more extensively applications. A few works to improve electrical conductivity of the Sb_2Se_3 nanomaterials have been reported.[9-12] For example, Donghyeuk et al. developed the Sb_2Se_3 nanowires decorated with Ag_2Se nanoparticles, which increased the electrical conductivity of the Sb_2Se_3 nanowires.[9] Zhang et al. explained an interpenetrating iodine-doped-Sb_2Se_3/Cu_2GeSe_3 heterojunction network fabricated by controlling the crystallization of a chalcogenide glass which can improve the photoelectric performance.[11]

During the past decades, considerable efforts have been devoted to the synthesis of one-dimensional Sb_2Se_3 nanostructures including nanorods, nanowires, nanotubes and nanoribbons by various methods, such as hydrothermal or solvothermal routes, surfactant or polymer-assisted hydrothermal technique, microwave irradiation method.[8, 12-16] However, the hydrothermal/solvothermal methods is generally time-consuming and needs additional protecting agents in order to obtain controlled morphology and dimension of the Sb_2Se_3 nanorods.[17] To the best of our knowledge, the synthesis of Sb_2Se_3 nanorods with colloid routes is relatively less investigated.[9, 18] Herein, we report an effective colloidal process involving hot-injection method for the high-quality synthesis of uniform single-crystal Sb_2Se_3 nanorods. Moreover, we firstly present an effective technique for directly preparing hybrid nanorods with $Sb_2Se_3/AgSbSe_2$ heterojunction structure. This interconnected heterojunction can significantly increase the electrical conductivity of the Sb_2Se_3 nanorods. The as-prepared hybrid nanorods with $Sb_2Se_3/AgSbSe_2$ heterojunction structure are directly used for fabricating prototype photodetectors, which demonstrates remarkable response to visible light. The possibility of using this new material concept for producing high-performance photodetector is also discussed.

[a] State Key Laboratory of Silicon Materials, School of Materials Science and Engineering, Zhejiang University, Hangzhou, 310027, P. R. China. E-mail: fanxp@zju.edu.cn
[b] Suzhou Institute of Nano-Tech and Nano-Bionics, Chinese Academy of Sciences (CAS), Suzhou, 215123, P. R. China
[c] Laboratory of Glasses and Ceramics, Institute of Chemistry, CNRS-Université de Rennes I, campus de Beaulieu, 35042 Rennes cedex, France
[d] College of Information Science and Electronic Engineering, Zhejiang University, Hangzhou, 310027, P. R. China

Electronic Supplementary Information (ESI) available: [details of any supplementary information available should be included here]. See DOI: 10.1039/x0xx00000x

Experimental section

Materials: Antimony acetate (Aladdin, 99.99%), Silver acetate (Aladdin, 99.5%), Selenium dioxide (Aladdin, 99%), 1-Hexadecylamine (Aladdin, 90%), 1-Octadecene (Aladdin, 90%) and Oleic acid (Aladdin, AR), Chloroform and Isopropyl alcohol were purchased from Sinopharm Chemical Reagent Co., Ltd. All reagents were used for the synthesis without further purification.

Synthesis of Sb_2Se_3 nanorods: A simple colloidal process involving hot-injection was used to synthesize one-dimensional Sb_2Se_3 nanorods. At first, 24 mmol selenium dioxide and 30 ml 1-octadecene were added into a 100 mL three-neck flask and heated to 200°C for several hours with stirring under argon atmosphere until selenium dioxide completely dissolved, which formed a 0.8 M selenium precursor solution. To prepare antimony precursor solution, 1 mmol antimony acetate, 8 mmol 1-hexadecylamine, 15 ml 1-octadecene and 6 ml oleic acid in another flask were degassed at room temperature and then heated to 220°C for 1 h, which formed a transparent yellow solution. Subsequently, 8 ml 0.8 M selenium precursor solution was swiftly injected into the yellow antimony precursor solution which was heated to 240°C beforehand. The mixture was stirred for 10 min and then cooled to room temperature. The obtained solid Sb_2Se_3 nanorods were collected by centrifugation, washed with chloroform and isopropyl alcohol for several times, and finally dried at 60°C under vacuum.

Synthesis of hybrid nanorods with $Sb_2Se_3/AgSbSe_2$ heterojunction structure: Two-step selenization process was used to synthesize the hybrid nanorods with $Sb_2Se_3/AgSbSe_2$ heterojunction structure. 2 ml 0.8 M selenium precursor solution was first swiftly injected into 240°C antimony precursor solution in the flask. Then 0.2 mmol silver acetate was added into the flask. After mixture was stirred for several minutes, another 6 ml 0.8 M selenium precursor was swiftly injected into the flask. The mixture was stirred for 10 minutes and then cooled to room temperature. The obtained hybrid nanorods with $Sb_2Se_3/AgSbSe_2$ heterojunction structure were collected by centrifugation, washed with chloroform and isopropyl alcohol for several times, and finally dried at 60°C under vacuum.

Characterization: XRD analysis was carried out on PAN alytical B.V. Empyrean 200895 x-ray diffractometer with Cu Kα radiation (λ = 1.54 Å), and scan speed was 2.00 deg/min. A Hitachi S-4800 field emission scanning electron microscope was used to observe the morphology. TEM, HRTEM, STEM images and the corresponding EDS mapping images were obtained from a FEI Tecnai G2F20 field emission transmission electron microscope operating at an acceleration voltage of 200 kV. Samples were prepared by placing a drop of a dilute chloroform dispersion of the nanorods on the surface of a copper grid. Energy dispersive spectroscopy (EDS) analysis has been performed with an EDAX instrument. The photoconductive performance of the photodetector were recorded using a Keithley 4200 SCS and SUSS PM8 probe station in a clean and shielded box at room temperature. A xenon lamp was used as the white light source for the photocurrent measurements. To further study the selective spectral response of the photodetectors, a monochromator was equipped, and the wavelength interval was set to 50 nm. The absorption spectra was taken from a SHIMADZU UV-3150 spectrophotometer. The Valence-band offset was analyzed by x-ray photoelectron spectroscopy (XPS, ESCALAB). The electrical properties were investigated by Hall-effect measurements using the Van der Pauw configuration (BID-RAD HL5500PC) at room temperature.

Results and discussion

Fig. 1a shows the XRD patterns of the Sb_2Se_3 nanorods, which exhibits prominent peaks in agreement with the JCPDS standard card (15-0861) of the orthorhombic phase of Sb_2Se_3 without a second phase, indicating the absence of any detectable impurities such as Se or Sb_2O_3 which could affect the optical and electrical properties. The SEM and TEM images

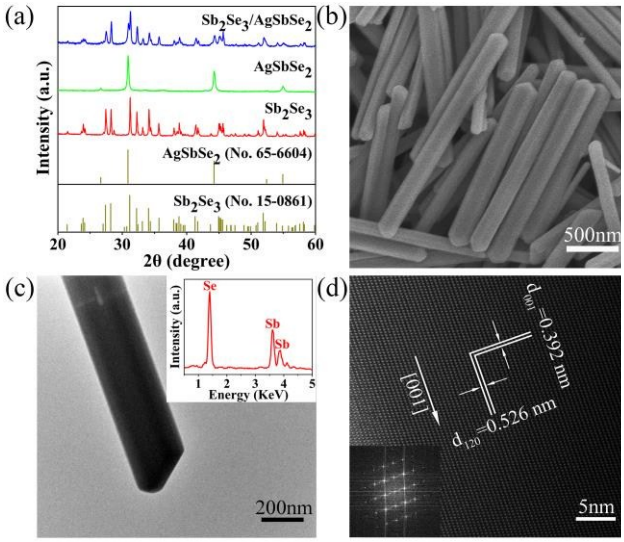

Fig. 1 (a) XRD patterns of Sb_2Se_3 nanorods, $AgSbSe_2$ nanoparticles and the hybrid nanorods with $Sb_2Se_3/AgSbSe_2$ heterojunction structure, (b) SEM image of Sb_2Se_3 nanorods, (c) TEM image and corresponding EDS spectrum (inset) of Sb_2Se_3 nanorod, (d) HRTEM image of Sb_2Se_3 nanorod, the bottom inset is a selected-area FFT.

(Fig. 1b-d) revealed the formation of highly uniform Sb_2Se_3 nanorods, with smooth surfaces throughout the entire length, a diameter of ~ 150-200 nm, and a typical length of several micrometers. An energy-dispersive x-ray spectrum (EDS, inset in Fig. 1c) of an individual nanorod exhibits strong Sb and Se peaks, and the atomic ratio of Sb and Se corresponds to the 2:3 stoichiometry within the precision of the measurements. HRTEM image and corresponding selected-area Fast Fourier Transform (FFT) pattern of a randomly selected nanorod (Fig. 1d) confirmed its highly crystalline nature with orthorhombic phase lattice fringes associated with (001) planes (*d*-spacing of 0.392 nm) appear along the nanorod, indicating that the nanorod grew along the [001] direction (c-axis). Moreover, the

XRD patterns of orthorhombic phase Sb_2Se_3 exhibit strong intensity of those (hk0) peaks, indicating that Sb_2Se_3 are preferentially grown along the (001) direction, which corresponds to the HRTEM result. According to the recent theoretical and experimental studies, the preferential growth is indeed determined intrinsically by the anisotropic Sb-Se atom chain or layer structure of orthorhombic Sb_2Se_3.[1, 19, 20] Photoconductivity is a well-known property of semiconductors which describes the electrical conductivity changes with the incident radiation. The photoconductive characteristics of the Sb_2Se_3 nanorods are investigated here by using the Sb_2Se_3 nanorods film-based photodetector. The interdigitated Au electrodes were fabricated on SiO_2/Si substrates using lithography (Fig. S1, Supporting Information).[21] Fig. 2a shows the I-V curves of the photodetector based on Sb_2Se_3 nanorods film. The electrical conductivity of the Sb_2Se_3 nanorods in dark condition is very low and similar to the bulk Sb_2Se_3 ($\sigma \sim 10^{-6}$-$10^{-2} \Omega^{-1}m^{-1}$). However, the device shows higher photosensitivity at different incident light densities, compared to bulk Sb_2Se_3. The photocurrent was significantly increased with increasing light intensity. To further investigate the photoresponse characteristics, a plot of time-resolved photoresponse at the bias of -10 V, -20 V and -30 V (incident light density of 12.05 mWcm^{-2}) is shown in Fig. 2b. When the applied voltage was -20 V, with the light irradiation on and off, the current across the nanorods film dramatically increases from -2 nA (OFF state, dark condition) to -100 nA (ON state, light illumination). The switching "ON/OFF" ratio is as high as 50, which is comparable to the very good results previously reported.[22] In addition, the response and the recovery times are other important parameters allowing to evaluate the speed of the ON/OFF switching processes. These two times are respectively defined as the time necessary for reaching 90% of the ΔI (ΔI is the difference between the maximum current and the minimum current) when the light is on and the time for returning from the maximum current to 10% of the ΔI. As shown in Fig. 2c and 2d, 0.7 s response and 1.1 s recovery times could be obtained, and the response and recovery times remained the same over 8 cycles, demonstrating the stability of the device. The Sb_2Se_3 nanorods used in this device were synthesized using a hot-injection method and were expected to be more resistant to oxidation and contained fewer surface defects. It is known that a superior crystal quality, the density of traps induced by defects is thus dramatically reduced and the photocurrent rapidly reaches a steady state both on rise and decay stages.[23] It is also noticed that the high photodetecting property of the nanorods is due to the high density of the surface sates inducing the depletion space charge layer. In Sb_2Se_3 nanorods, a depletion space charge layer forms due to the surface state and Fermi-level pinning, which allows for physical separation of the electron and hole. It has reported that when the critical diameter is reached, the depletion layer remains fully depleted and the recombination barrier increases and may further increase the photocurrent as the nanorods diameter increases.[9, 24] Therefore, the high photodetecting property of the Sb_2Se_3 nanorods could also be attributed to the larger diameter of Sb_2Se_3 nanorods (~150-200 nm).

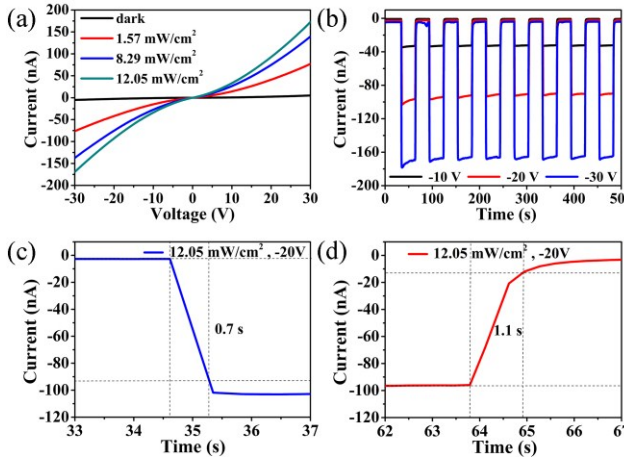

Fig. 2 Photoconductive performance of the photodetector based on the Sb_2Se_3 nanorods film. (a) Dark current and photocurrents at different incident power densities, (b) Time-resolved photoresponse at the bias of -10 V, -20 V and -30 V with an incident light density of 12.05 mWcm^{-2}, Demonstration of (c) the response speed and (d) the recovery speed at a bias of -20 V and an incident light density of 12.05 mWcm^{-2}.

It is well known that the Sb_2Se_3 has a high absorption coefficient and very low electrical conductivity. To fabricate more efficient photodetectors, the electrical conductivity of the Sb_2Se_3 nanorods should be efficiently improved. The $AgSbSe_2$ is one important ternary semiconductor from the I-V-VI family, shows an excellent electrical conductivity of 154 $\Omega^{-1}cm^{-1}$.[25-28] In addition to this prominent intrinsic property, $AgSbSe_2$ is a narrow band gap semiconductor (~1 eV) with a favourable valence band structure composed of multiple flat valleys, favourable for electrical conductivity improvement through doping or by forming functional junctions.[29, 30] The $AgSbSe_2$ nanoparticles were synthesized via a similar colloidal chemical process (Supporting Information). The as-synthesized $AgSbSe_2$ nanoparticles correspond to the cubic structure (Fig. 1a). The TEM image (Fig. S2a, Supporting Information) shows that the nanoparticles have a quasi-spherical morphology with diameters between 10 and 25 nm. The photodetector based on the $AgSbSe_2$ nanoparticles film exhibited much higher dark current and photocurrent in comparison with that based on the Sb_2Se_3 nanorods film (Fig. S2b, Supporting Information). To improve the performance of the photodetectors based on Sb_2Se_3 nanorods film, we developed a two-step selenization method to synthesize the hybrid nanorods with Sb_2Se_3/$AgSbSe_2$ heterojunction structure. The XRD pattern of the hybrid nanorods with Sb_2Se_3/$AgSbSe_2$ heterojunction structure (Fig. 1a) shows that all diffraction peaks can match very well with the standard card of Sb_2Se_3 (JCPDS 15-0861) or $AgSbSe_2$ (JCPDS 65-6604) without any visible peak of impurities.

Fig. 3 shows the SEM, TEM, HRTEM, STEM and the corresponding EDS mapping images of the hybrid nanorods. Some small nanoparticles incorporated onto the nanorods can be observed. The representative HRTEM images obtained from

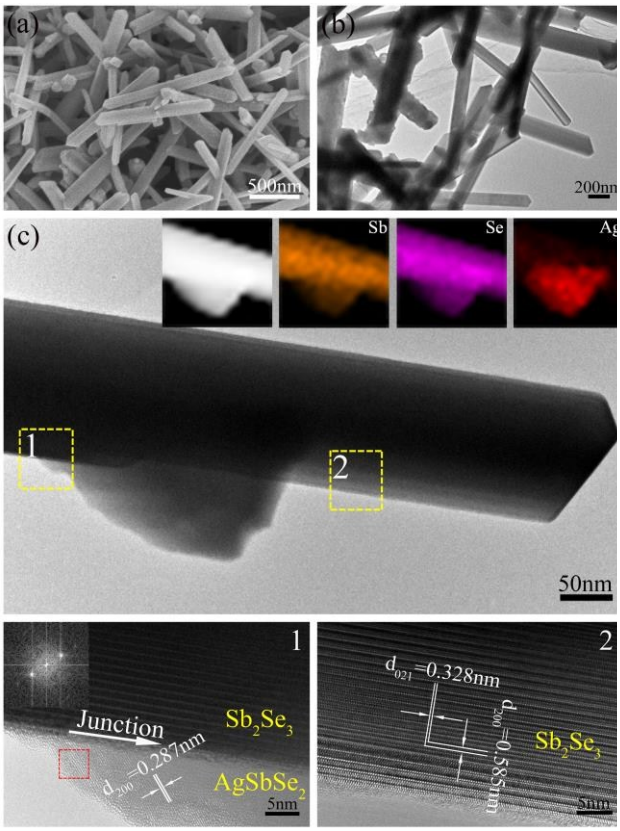

Fig. 3 Structural and morphological characterization of the hybrid nanorods with $Sb_2Se_3/AgSbSe_2$ heterojunction structure. (a) SEM image, (b) TEM image, (c) TEM image and HRTEM images from the selected areas 1 and 2 of an individual hybrid nanorod (Inset in the left HRTEM image is a FFT pattern from the red marked area), the inset of (c) shows a STEM image and the corresponding EDS mapping images of Sb, Se and Ag elements, respectively.

the selected areas 1 and 2 of Fig. 3c show that the nanoparticle and the nanorod have different lattice structures and a visible interface. The interplanar d-spacing of 0.287 nm correspond to the (200) plane of $AgSbSe_2$, the selected-area Fast Fourier Transform (FFT) pattern (inset in the left HRTEM image) from the red marked area further confirms the $AgSbSe_2$ crystalline phase. The interplanar d-spacings of 0.585 nm and 0.328 nm agree well with the distance of the (200) lattice plane and (021) lattice plane of Sb_2Se_3, respectively. The EDS mapping images showed the Sb and Se atoms were distributed in both the nanorod and the nanoparticles. However, Ag distribution was restricted to the specific areas corresponding to the position of the nanoparticles and to a small part of the nanorod near to the nanoparticles, which indicated the formation of $AgSbSe_2$ nanoparticles on the surface of the Sb_2Se_3 nanorod. It is obvious that the nanoparticles belong to $AgSbSe_2$ phase (pure $AgSbSe_2$ nanoparticles were synthesized, as shown in Fig. S2a, Supporting Information) and the nanorods to Sb_2Se_3 phase.

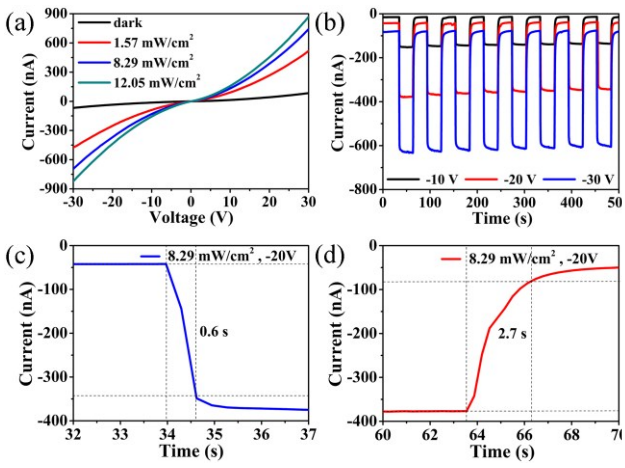

Fig. 4 Photoconductive performance of the photodetector based on the $Sb_2Se_3/AgSbSe_2$ hybrid nanorods film. (a) Dark current and photocurrents at different incident power densities, (b) Time-resolved photoresponse at the bias of -10 V, -20 V and -30 V with an incident light density of 8.29 mW cm^{-2}, (c) Response speed and (d) the recovery speed at a bias of -20 V.

Fig. 4 shows the photoconductive performance of the photodetector based on the $Sb_2Se_3/AgSbSe_2$ hybrid nanorods film. Compared with the photodetector based on the Sb_2Se_3 nanorods film, the current under dark conditions increased approximately 20 times (from -2 nA to -40 nA at -20 V) and the photocurrent increased approximately 4.5 times (from -100 nA to -450 nA at -20 V, 12.05 $mWcm^{-2}$). A useful figure of merit for the photodetector is the responsivity (R_{res}), which can be calculated from:

$$R_{res}=I_{ph}/I_{irr}A \quad (1)$$

where I_{ph} is the background substituted photocurrent ($I_{illumination}$-I_{dark}), I_{irr} is the irradiance of the incident light, and A is the effective device area.[22, 31, 32] The R_{res} of the photodetector based on the $Sb_2Se_3/AgSbSe_2$ hybrid nanorods film can be calculated to be about 4.2 times as much as that of the photodetector based on the Sb_2Se_3 nanorods film. As shown in Fig. 3a, $AgSbSe_2$ nanoparticles grew on the surface of Sb_2Se_3 nanorods, leading to the formation of a $Sb_2Se_3/AgSbSe_2$ heterojunction. The $AgSbSe_2$ nanoparticles with higher electrical conductivity might connect to each other along the rod orientation, thereby improving the electrical conductivity of the $Sb_2Se_3/AgSbSe_2$ hybrid nanorods and eventually increasing the electrical conductivity under dark. To further confirm the results, hall-effect measurement was carried out to examine the electrical properties of the as-synthesized Sb_2Se_3 nanorods, $AgSbSe_2$ nanoparticles and $Sb_2Se_3/AgSbSe_2$ hybrid nanorods. The typical values were shown in Table S1 (Supporting Information). It can be seen that Sb_2Se_3 exhibits a weak p-type conductivity with the lower carrier concentration. Compared with Sb_2Se_3 nanorods, the electrical conductivity for the $Sb_2Se_3/AgSbSe_2$ hybrid nanorods have a significant improvement with several orders of magnitude, which accurately corresponds to the results as shown in

photodetector. Previous studies have revealed that the formation of ZnO/α-Fe_2O_3 semiconductor nanoheterostructures significantly enhances the electrical conductivity.[33] In this work, when the Sb_2Se_3/$AgSbSe_2$ heterojunction was formed, the free electrons from $AgSbSe_2$ nanoparticles can easily migrate to the Sb_2Se_3 nanorods due to the potential difference at the heterojunction interface. Moreover, the formation of the heterojunction resulted in more effective interfacial charge separation and the higher carrier concentration, which could significantly enhance the electrical conductivity of the hybrid nanorods with Sb_2Se_3/$AgSbSe_2$ heterojunction. Thus the photo-generated carriers can be transported efficiently through the conductive channels in the nanorods film. In addition, the light absorption efficiency can be increased in the hybrid nanorods by particle induced light scattering.[32] It is obvious that the improved light absorption efficiency and the higher electrical conductivity will significantly increase the photocurrent of the Sb_2Se_3/$AgSbSe_2$ hybrid nanorods.

Fig. 4c and 4d give the response/recovery times of 0.6/2.7 s for light intensity of 8.29 $mWcm^{-2}$ at a bias of -20 V. These performances are stable even after 8 cycles, demonstrating the excellent photoresponse stability of the photodetector based on the Sb_2Se_3/$AgSbSe_2$ hybrid nanorods film. It is obvious that this photodetector has balanced the conductivity and the photo responsivity. The demonstrated performances

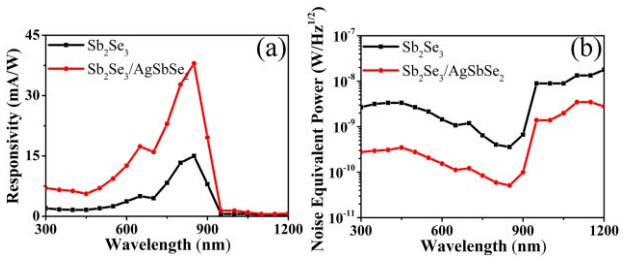

Fig. 5 Wavelength-dependent (a) responsivity and (b) noise equivalent power (NEP) of the photodetectors at a bias of -20 V.

make it a promising candidate for applications as high-performance photodetectors.

To clearly show the selective spectral response of the photodetectors, photodetecting at the monochromatic wavelength in range from UV to IR was studied. Fig. 5a shows the wavelength-dependent responsivity (R_{res}) of the photodetectors based on Sb_2Se_3 nanorods film and Sb_2Se_3/$AgSbSe_2$ hybrid nanorods film. These two photodetectors show a similar selective response with a broad spectral response from 450 nm to 950 nm, and reach the highest responsivity at 850 nm. The R_{res} values of the photodetector based on the Sb_2Se_3/$AgSbSe_2$ hybrid nanorods film can be calculated to be about 3-4 times as much as that of the photodetector based on the Sb_2Se_3 nanorods film, and the values are comparable to some reported inorganic photodetectors.[34] To further characterize the performance of these photodetectors, it is important to determine the noise characteristics. The noise equivalent power (NEP), which is the incident power at which the signal is equal to the RMS dark noise density (S_I), measured within a specified bandwidth (commonly 1 Hz), that is, NEP=S_I/R_{res}.[35] To obtain S_I, a large sequence of current fluctuations (I_{noise}) was measured with 0.5 s integration time (which corresponds to a bandwidth of 1 Hz), while keeping the photodetectors in darkness. The RMS noise density was then calculated as $S_I=(\langle I^2_{noise}\rangle/1\ Hz)^{1/2}$. The obtained NEP across the working spectrum is shown in Fig. 5b. It was found that the NEP can reach 4×10^{-10} $W/Hz^{1/2}$ for the photodetector based on Sb_2Se_3 nanorods film and 5×10^{-11} $W/Hz^{1/2}$ for the photodetector based on Sb_2Se_3/$AgSbSe_2$ hybrid nanorods film at 850 nm. It is worthwhile to note that a weak incidence can

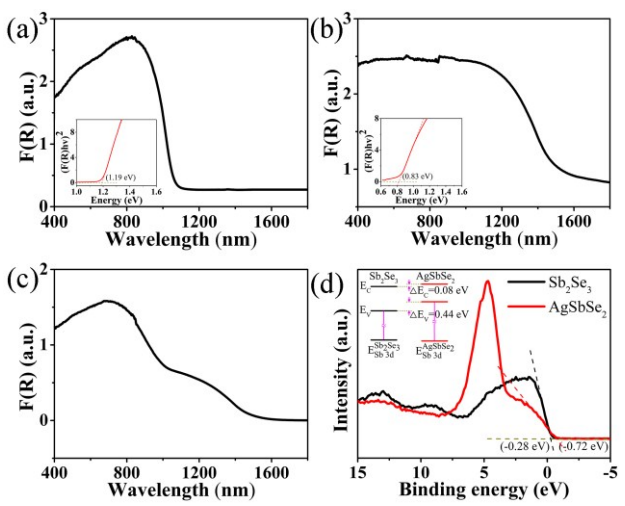

Fig. 6 (a) Optical absorption spectra (calculated from diffuse reflectance data) for Sb_2Se_3 nanorods. Inset: A plot of $[F(R)hv]^2$ vs. energy for the Sb_2Se_3 nanorods, from which direct band gap energy was obtained, (b) Absorption spectra for $AgSbSe_2$ nanoparticles. Inset: A plot of $[F(R)hv]^2$ vs. energy, (c) Absorption spectra for the hybrid nanorods with Sb_2Se_3/$AgSbSe_2$ heterojunction, (d) Valence-band edge (VBE) spectra for Sb_2Se_3 nanorods and $AgSbSe_2$ nanoparticles. Inset: Schematic diagram of type-II band alignment of the heterojunction.

be detected above the noise level, and the NEP values of our photodetectors are comparable to that of state-of-the-art devices.[36]

Analysis of optical absorption spectra is one of the most effective tools for understanding and/or engineering the band structure and energy gaps of semiconductor materials. It is known that proper band-gap of semiconductor is important to fabricate the high performance photodetectors. In this work, optical absorption spectra has been used to investigate the optical properties of the as-synthesized Sb_2Se_3 nanorods, $AgSbSe_2$ nanoparticles and the hybrid nanorods with Sb_2Se_3/$AgSbSe_2$ heterojunction. Herein, the absorption data were calculated from diffuse reflectance data using Kubelka–Munk equations: $F(R)=\alpha/\Lambda=(1-R)^2/(2R)$, where R is the reflectance, α and Λ are the absorption and scattering coefficients, respectively.[37] As shown in Fig. 6a, the onset of

absorption for Sb_2Se_3 nanorods starts near 1100 nm. A plot of $[F(R)hv]^2$ versus energy (hv) yielded a direct band gap of 1.19 eV (inset in Fig. 6a). Similarly, Fig. 6b shows that the onset of absorption for $AgSbSe_2$ nanoparticles starts near 1600 nm and the corresponding direct band gap is 0.83 eV. The absorption spectrum of the hybrid nanorods with $Sb_2Se_3/AgSbSe_2$ heterojunction (Fig. 6c) exhibits two optical absorption peaks, and the onsets match very well with $AgSbSe_2$ and Sb_2Se_3, respectively. To further investigate the band offset of $Sb_2Se_3/AgSbSe_2$ heterojunction, x-ray photoelectron spectroscopy (XPS) has been extensively employed, which lies on a core-level photoemission-based method, using a linear extrapolation method to determine the valence band maximum.[38, 39] The valence-band offset (ΔE_V) is obtained by the following expression:

$$\Delta E_V=(E_{Sb\text{-}3d}-E_V)_{Sb_2Se_3}-(E_{Sb\text{-}3d}-E_V)_{AgSbSe_2}-(E_{Sb\text{-}3d}-E_{Sb\text{-}3d})_{Sb_2Se_3/AgSbSe_2} \quad (2)$$

According to the Sb-3d x-ray photoelectron spectroscopy (Fig. S3, Supporting Information) and the valence-band edge (VBE) spectra (Fig. 6d), the ΔE_V is calculated to be 0.44 eV, and the conduction-band offset is deduced to be 0.08 eV. It was found that $Sb_2Se_3/AgSbSe_2$ heterojunction has a type-II band alignment (inset in Fig. 6d). Accordingly, as a direct band gap semiconductor, the experimental band gaps for the as-synthesized semiconductors are close to the optimum value for photovoltaic conversion, implying their promising applications in photoelectric devices, including high performance photodetectors.

Conclusions

An effective colloidal process involving hot-injection method has been developed for the synthesis of uniform single-crystalline Sb_2Se_3 nanorods with an average diameter of ~ 150-200 nm. The photoconductive characteristics of the as-synthesized Sb_2Se_3 nanorods are investigated by developing a film-based photodetector. The device displayed a remarkable response to visible light intensity with an "ON/OFF" ratio as high as 50, short response/recovery times and long-term durability. In order to overcome the challenge of intrinsic low electrical conductivity of Sb_2Se_3, the hybrid nanorods with $Sb_2Se_3/AgSbSe_2$ heterojunction structure are firstly prepared. Thanks to the excellent electron transport ability and to an increase in the charge collection capability, the electric current of the photodetector based on the $Sb_2Se_3/AgSbSe_2$ hybrid nanorods film is increased approximately by 20 times in dark and 4.5 times under light illumination. The responsivity of the photodetector based on the $Sb_2Se_3/AgSbSe_2$ hybrid nanorods film is about 4.2 times as much as that of the photodetector based on the Sb_2Se_3 nanorods film. The exact band gap of the Sb_2Se_3 nanorods and $AgSbSe_2$ nanoparticles are experimentally defined to 1.19 eV and 0.83 eV respectively, the heterojunction has a type-II band alignment and its valence-band offset is determined to be 0.44 eV. These demonstrated performances make the hybrid nanorods with $Sb_2Se_3/AgSbSe_2$ heterojunction structure a promising material/concept for designing highly sensitive photodetectors.

Acknowledgements

The authors gratefully acknowledge support for this research from the Program for Innovative Research Team in University of Ministry of Education of China (IRT13R54) and the Fundamental Research Funds for the Central Universities (2015FZA4008).

Notes and references

1 Y. Zhou, L. Wang, S. Chen, S. Qin, X. Liu, J. Chen, D.-J. Xue, M. Luo, Y. Cao, Y. Cheng, E. H. Sargent and J. Tang, *Nat Photon*, 2015, **9**, 409-415.
2 Y. Shirasaki, G. J. Supran, M. G. Bawendi and V. Bulović, Nature Photonics, 2012, 7, 13-23.
3 F. Huang, J. Zhou, J. Xu and Y. Wang, *Nanoscale*, 2014, **6**, 2340-2344.
4 J. N. Freitas, A. S. Goncalves and A. F. Nogueira, *Nanoscale*, 2014, **6**, 6371-6397.
5 J. van Embden, K. Latham, N. W. Duffy and Y. Tachibana, *Journal of the American Chemical Society*, 2013, **135**, 11562-11571.
6 C. Xiao, J. Xu, B. Cao, K. Li, M. Kong and Y. Xie, *Journal of the American Chemical Society*, 2012, **134**, 7971-7977.
7 R. Vadapoo, S. Krishnan, H. Yilmaz and C. Marin, *Nanotechnology*, 2011, **22**, 175705.
8 J. Ota and S. K. Srivastava, *Optical Materials*, 2010, **32**, 1488-1492.
9 D. Choi, Y. Jang, J. Lee, G. H. Jeong, D. Whang, S. W. Hwang, K. S. Cho and S. W. Kim, *Scientific reports*, 2014, **4**, 6714.
10 R. C. Jin, G. Chen, J. Pei, J. X. Sun and Y. Wang, *Nanoscale*, 2011, **3**, 3893-3899.
11 X. H. Zhang, Y. Xu, Q. H. Shen, B. Fan, X. S. Qiao, X. P. Fan, H. Yang, Q. Luo, L. Calvez, H. L. Ma, M. Cathelinaud and J. J. Simond, *Journal of Materials Chemistry A*, 2014, **2**, 17099-17106.
12 R. Jin, G. Chen, Q. Wang, J. Sun and Y. Wang, *Journal of Materials Chemistry*, 2011, **21**, 6628.
13 J. Ma, Y. Wang, Y. Wang, P. Peng, J. Lian, X. Duan, Z. Liu, X. Liu, Q. Chen, T. Kim, G. Yao and W. Zheng, *CrystEngComm*, 2011, **13**, 2369.
14 C. Zhao, X. Cao and X. Lan, *Materials Letters*, 2007, **61**, 5083-5086.
15 L. Guo, G. Ji, X. Chang, M. Zheng, Y. Shi and Y. Zheng, *Nanotechnology*, 2010, **21**, 035606.
16 G. Y. Chen, B. Dneg, G. B. Cai, T. K. Zhang, W. F. Dong, W. X. Zhang and A. W. Xu, *Journal of Physical Chemistry C*, 2008, **112**, 672-679.
17 J. M. Ma, Y. P. Wang, Y. J. Wang, Q. Chen, J. B. Lian and W. J. Zheng, *Journal of Physical Chemistry C*, 2009, **113**, 13588-13592.
18 Z. T. Deng, M. Mansuripur and A. J. Muscat, *Nano letters*, 2009, **9**, 2015-2020.
19 D. Wang, D. Yu, M. Mo, X. Liu and Y. Qian, *Journal of Crystal Growth*, 2003, **253**, 445-451.
20 D. B. Wang, C. X. Song, X. Fu and X. Li, *Journal of Crystal Growth*, 2005, **281**, 611-615.
21 Y.-Q. Liu, M. Zhang, F.-X. Wang and G.-B. Pan, *Journal of Materials Chemistry C*, 2014, **2**, 240.
22 G. A. O'Brien, A. J. Quinn, D. A. Tanner and G. Redmond, *Advanced materials*, 2006, **18**, 2379-2383.
23 T. Y. Zhai, X. S. Fang, M. Y. Liao, X. J. Xu, L. Li, B. D. Liu, Y. Koide, Y.

Ma, J. N. Yao, Y. Bando and D. Golberg, *Acs Nano*, 2010, **4**, 1596-1602.
24 R. Calarco, M. Marso, T. Richter, A. I. Aykanat, R. Meijers, A. V. Hart, T. Stoica and H. Luth, *Nano letters*, 2005, **5**, 981-984.
25 S. Berri, D. Maouche and Y. Medkour, *Physica B: Condensed Matter*, 2012, **407**, 3320-3327.
26 K. Bindu, M. T. S. Nair, T. K. Das Roy and P. K. Nair, *Electrochemical and Solid State Letters*, 2006, **9**, G195-G199.
27 K. Wojciechowski, J. Tobola, M. Schmidt and R. Zybala, *Journal of Physics and Chemistry of Solids*, 2008, **69**, 2748-2755.
28 S. N. Guin, A. Chatterjee, D. S. Negi, R. Datta and K. Biswas, *Energy & Environmental Science*, 2013, **6**, 2603.
29 S. N. Guin, D. S. Negi, R. Datta and K. Biswas, *Journal of Materials Chemistry A*, 2014, **2**, 4324-4331.
30 S. N. Guin and K. Biswas, *Chemistry of Materials*, 2013, **25**, 3225-3231.
31 A. Iwasaki, L. Hu, R. Suizu, K. Nomura, H. Yoshikawa, K. Awaga, Y. Noda, K. Kanai, Y. Ouchi, K. Seki and H. Ito, *Angewandte Chemie-International Edition*, 2009, **48**, 4022-4024.
32 W. Wang, X. Lu, Z. Li, X. Li, X. Xu, J. Lei, C. Wang, R. H. Baughman and S. Fang, *Organic Electronics*, 2012, **13**, 2319-2325.
33 D. Sarkar, G. G. Khan, A. K. Singh and K. Mandal, *The Journal of Physical Chemistry C*, 2012, **116**, 23540-23546.
34 Y. Xie, M. G. Gong, T. A. Shastry, J. Lohrman, M. C. Hersam and S. Q. Ren, *Advanced materials*, 2013, **25**, 3433-3437.
35 X. An, F. Liu, Y. J. Jung and S. Kar, *Nano letters*, 2013, **13**, 909-916.
36 H. Wei, Y. Fang, Y. Yuan, L. Shen and J. Huang, *Advanced materials*, 2015, **27**, 4975-4981
37 D. D. Vaughn, R. J. Patel, M. A. Hickner and R. E. Schaak, *Journal of the American Chemical Society*, 2010, **132**, 15170-15172.
38 R. Deng, B. Yao, Y. F. Li, Y. M. Zhao, B. H. Li, C. X. Shan, Z. Z. Zhang, D. X. Zhao, J. Y. Zhang, D. Z. Shen and X. W. Fan, *Applied Physics Letters*, 2009, **94**, 022108.
39 S. C. Su, Y. M. Lu, Z. Z. Zhang, C. X. Shan, B. H. Li, D. Z. Shen, B. Yao, J. Y. Zhang, D. X. Zhao and X. W. Fan, *Applied Physics Letters*, 2008, **93**, 082108.